water

MDPI

Article

Ubiquitous Fractal Scaling and Filtering Behavior of Hydrologic Fluxes and Storages from A Mountain Headwater Catchment

Ravindra Dwivedi [1,2,*], John F. Knowles [3,4], Christopher Eastoe [5], Rebecca Minor [4,6], Nathan Abramson [1], Bhaskar Mitra [7,8], William E. Wright [9], Jennifer McIntosh [1], Thomas Meixner [1], Paul A. "Ty" Ferre [1], Christopher Castro [1], Guo-Yue Niu [1], Greg A. Barron-Gafford [4,6], Michael Stanley [10] and Jon Chorover [11]

S1. Using Z-Score vs. Scaled Hyperbolic Arcsine Transformation Function to Transform A Time Series

It is a standard practice in harmonic time series analysis to use either z-scores, if a time series is normally distributed, or the Standardized Precipitation Index (SPI-method), if a time series is skewed (e.g., precipitation) [1,2]. In the z-score method, a time series is transformed by first subtracting the sample mean value and then dividing by one sample standard deviation. If a time series is normally distributed, this method is acceptable for equalizing variance throughout the time series. In the SPI-method, a skewed time series (e.g., a time series whose probability density function can be approximated as a gamma distribution skewed to the right) is transformed into a standard normal distribution through equiprobability transformation (see Edwards [3] for method details) and variance is then equalized using z-scores.

Using both Kolmogorov-Smirnov and Lilliefors tests, we found that none of the standardized distributions for hydrologic fluxes (Figure S1) were normally distributed at the 95% confidence level [4]. Before performing either test, each time series was transformed by using the sample mean and one sample standard deviation of the corresponding time series. Subsequently, the built-in functions *kstest* and *lillietest* in MATLAB® were used for performing Kolmogorov-Smirnov and the Lilliefors tests, respectively. We rejected the null hypothesis that a time series was obtained from data composing a standard normal distribution when $p < 0.001$ for both tests in the case of precipitation, streamflow, actual evapotranspiration (AET), and daily changes in soil and bedrock storage.

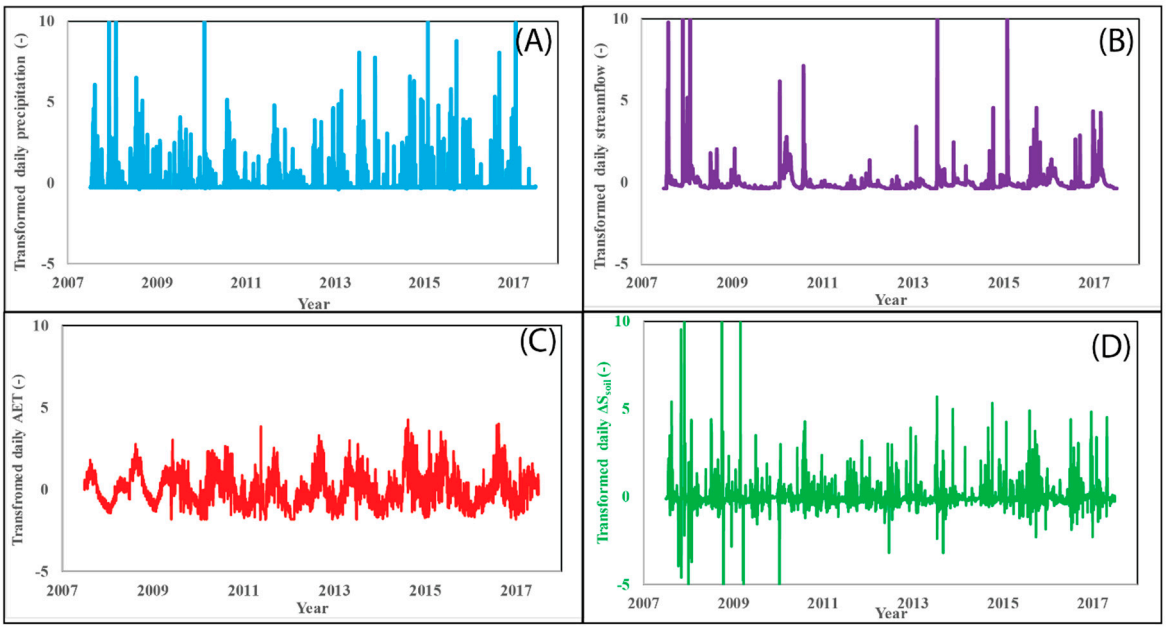

Figure S1. Transformed time series data of catchment-scale precipitation (**A**), streamflow (**B**), AET (**C**), and soil water storage (**D**) from water year (WY) 2008 through WY 2017 (water year n is defined as 1 July of calendar year n-1 to 30 June of year n). Note: (i) the maximum y-axis value for the plot (A) is 22 (dimensionless; shown here by the symbol "-"), but the y-axis is restricted to 10 (dimensionless) to aid visualization; (iii) the maximum y-axis value for the plot (B) is 34 (dimensionless), but the y-axis is restricted to 10 (dimensionless) to aid visualization; and (iv) the minimum and maximum y-axis values for the y-axis in the plot (D) are -23 (dimensionless) and 32 (dimensionless) respectively, but the axis is restricted to -5 (dimensionless) to 10 (dimensionless) to aid visualization.

S2. Optimal Time Series Transformation of Streamflow Data

We used a scaled arcsine hyperbolic transformation function (Equation 2 in the main text or Equation S1 below) in order to equalize the variance of daily hydrologic and subsurface storage time series data Kirchner and Neal [5]. The variance-equalizing property of this function depends on the base value that is used to normalize the time series, i.e., A_{ref} in Equation S1 (Dr. J. Kirchner, Personal communication, 2017). We therefore performed a sensitivity analysis on A_{ref} by selecting A_{ref} values equal to the sample mean, median, and maximum of each time series (we did not include the minimum value of streamflow for A_{ref} as this value is zero at MGC). For comparison purposes, the natural log-transformed daily streamflow was also included in our analysis. Our results (see Figure S2) suggest that a scaled arcsine hyperbolic transformation with A_{ref} equal to the sample median provided a better equalization of variance than the natural log-transformation or scaled arcsine hyperbolic transformations using mean or maximum of A_{ref}. As a result, the hydrologic flux and subsurface storage time series data in this work were transformed using a scaled arcsine hyperbolic transformation (Equation (S1)) with A_{ref} set to equal the sample median.

$$A_{tra}(t) = \log_e\left(\frac{A(t)}{A_{ref}} + \sqrt{1 + \left(\frac{A(t)}{A_{ref}}\right)^2}\right), \quad \text{(S1)}$$

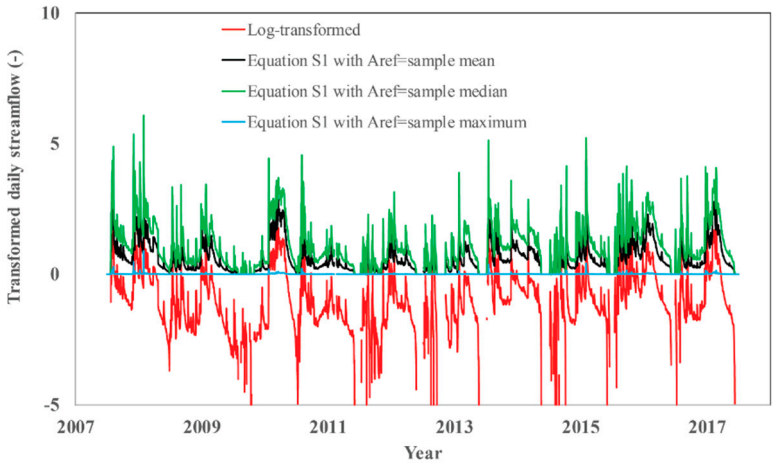

Figure S2. Transformed daily streamflow using various transformation bases (A_{ref}). Note: (i) the red curve is drawn using the standard $\log_e$ transformation of non-zero daily streamflows and (ii) black, green and blue curves are drawn using the arcsine transformation function (Equation S1) with A_{ref} values corresponding to the sample mean, median, and maximum values, respectively.

S3. Effect of Missing Values and Methodology for Estimating the Power Spectrum of A Normal Random Time Series

Our method for estimating the power spectrum of a time series with data gaps includes the following steps: (a) alias filtering, (b) spectral smoothing, and (c) selecting a spectral analysis method. We used a Kirchner filter in order to reducing spectral aliasing effects [6]. The input to the Kirchner filter is the corner frequency, which is the frequency at which the power spectrum of a time series steepens significantly [5]. To estimate the corner frequency, we first plotted streamflow at hourly intervals (Figure S3) for the first 500 hours of calendar year 2007. Subsequently, we estimated the time interval below which the variability in the streamflow time series was significantly reduced in the sense that streamflow varied smoothly below that time scale (see Kirchner and Neal [5] for more details), which was equal to two hours for streamflow at MGC. The corner frequency with the 2-hour time interval, or with a wavelength of 4-hr, was 2190 cycles per year (cpy). Note that the importance of specifying the exact value of this corner frequency depends on the power spectrum of a time series and on the sampling frequency [6]. For example, if the corner frequency is significantly higher than the sampling frequency (which is 365 cpy when using daily observations), the power spectrum of a time series is not significantly affected by the exact value of the specified corner frequency. However, if the corner frequency is very close to the sampling frequency, then the exact value of the specified corner frequency affects the power spectrum of a time series e.g., Figure 7e in Kirchner [6]. In our study, we used a fixed corner frequency of 2190 cpy when filtering the power spectrum of a time series in order to reduce the potential for spectral aliasing effects.

Due to our use of daily averaged data in place of instantaneous values in this study, it is expected that the power spectra of the daily averaged fluxes and storage time series data would be less affected by spectral aliasing effects relative to the instantaneous values [6].

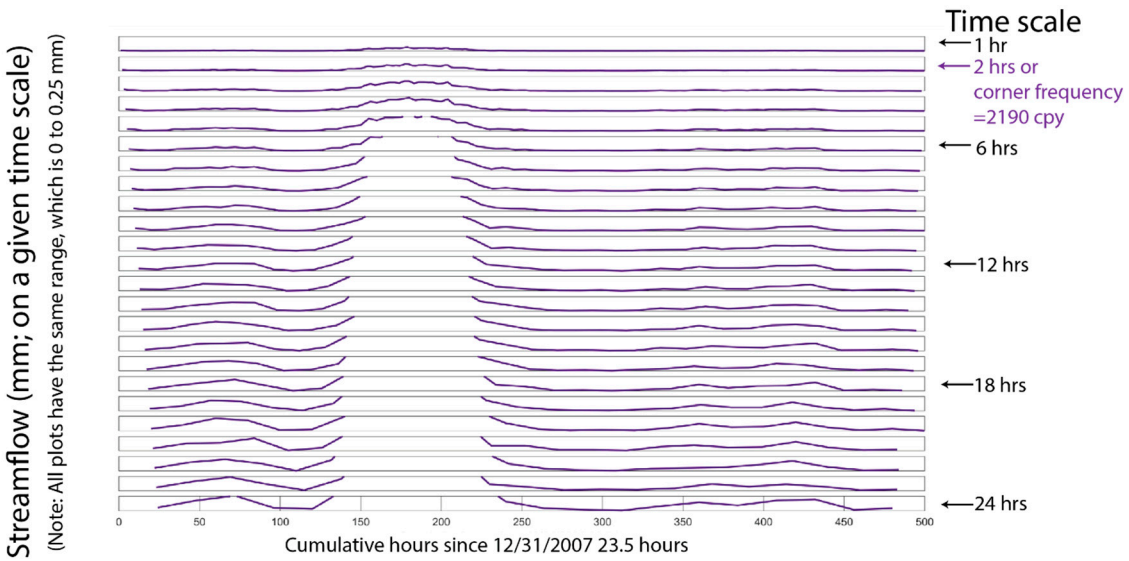

Figure S3. Hourly plot of the streamflow data for the first 500 hours for the calendar year 2007. In our presentation of hourly streamflows, the hourly streamflows are selected on the hourly time intervals from 30-minute time interval time series rather than being estimated as an average of two 30-minute consecutive values. cpy: cycles per year.

In this work, we selected the weighted wavelet transform (WWT) method to estimate the power spectra of time series data with uneven time steps. The WWT method was chosen in favor of the Lomb-Scargle (LS; see Kirchner, et al. [7]) or Date Compensated Discrete Fourier transform (DCDFT; see Godsey, et al. [8]) methods as it is better able to reduce spectral leakage from power associated with long-period signals to power associated with low-period signals [5]. However, we compared the skill of multiple methods including the Discrete Fourier Transform (DFT), DCDFT, and WWT methods for continuous time series data, and the LS, DCDFT, and WWT methods for time series data with gaps, at estimating the power spectra of a normal random time series with mean zero and variance one. The purpose of this evaluation was to better understand the effects of our method selection, specifically with respect to spectral smoothing and alias filtering. Note that the power spectrum of a normal random time series is expected to be a white noise spectrum, i.e., it is expected to have a slope of zero. To more completely understand the effect of data gaps on the resultant power spectra, some data gaps in the time series were intentionally created by deleting values so that the time series resembled some the observed time series for $\delta^{18}O$ in precipitation and stream water (Figures 2A and B). We used the interval WY 2008 and WY 2012, the same interval for which time series data in precipitation and stream waters were available.

For a normal random time series without any data gaps (Figure S4A1), alias filtering of the power spectrum resulted in a non-zero slope (which should otherwise be zero) using the DFT or DCDFT (not shown) methods but not the WWT method (Figure S4). With the DFT (or DCDFT) method and without any alias filtering (see Figure S4B1), the slope of the power spectrum for the normal random time series was approximately zero. However, when alias filtering was performed using the DFT method on the same time series, the slope of the power spectrum was neither zero nor approximately zero (Figure S4B2). Spectral smoothing of the power spectrum amplified this trend regardless of which method was used (Figure S4B3 vs. B2), but the non-zero spectral slope persisted when taking the ratio of the power spectra of any two normal random time series' with the DFT (or the DCDFT method) method (black curve in Figure S4B4). The power spectrum of a normal random time series with or without alias filtering resulted in a slope of approximately zero with the WWT method (red curves in Figures S4A through D).

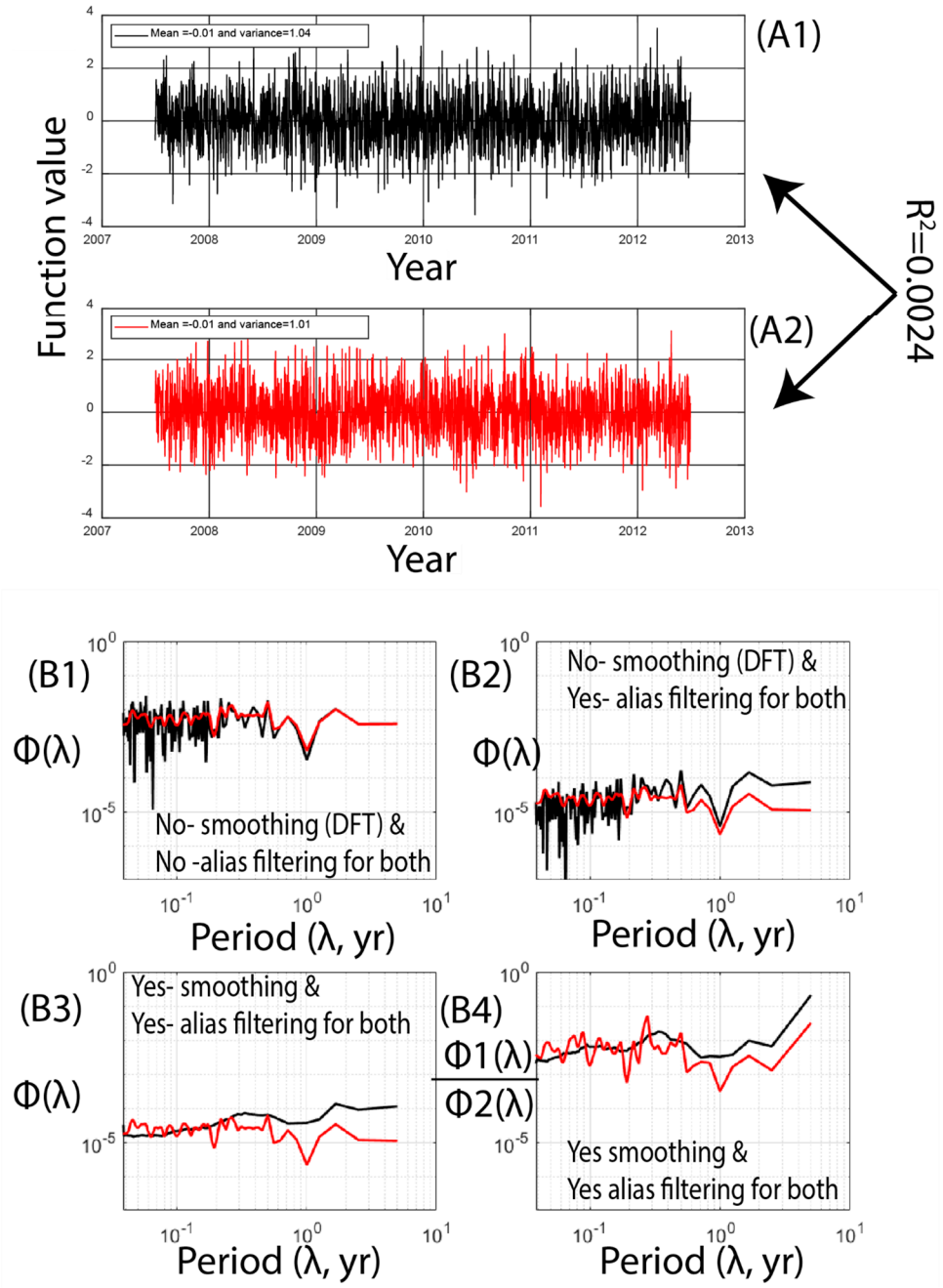

Figure S4. Effect of spectral smoothing and alias filtering on the power spectra of a continuous normal random time series (A1) using the Discrete Fourier Transform method (DFT; shown in black), and (A2) on another continuous normal random time series using the Weighted Wavelet Transform (WWT; shown in red) method. (B1) Power spectra generated with the DFT and WWT methods without power spectral smoothing for DFT and without alias filtering for both methods. (B2) Power spectra generated with the DFT and WWT methods without power spectral smoothing for DFT, but with alias filtering both methods. (B3) Power spectra generated with the DFT and WWT methods with both power spectral smoothing and alias filtering for both methods. (B4) The ratio of the power spectra of time series A1 and A2 using DFT (shown in black) and between time series A1 and A2 using WWT (shown in red), with both power spectral smoothing and alias filtering for both methods. Note that the expected power spectrum is a constant for a normal random process, and that the power spectra generated using the Date Compensated Discrete Fourier Transform (DCDFT) method were very similar to the power spectra obtained using DFT.

For normal random time series data with intentionally created data gaps (Figure S5A1), the slopes of the power spectra generated using the LS and WWT methods were approximately zero when they were not alias-filtered (Figure S5B1). However, when the power spectrum for a normal random time series with the LS method was alias filtered, the spectral slope was non-zero (Figure S5B2), and this trend was enhanced by spectral smoothing (see Figure S5B3 vs. S5B2). As for DFT analysis, taking the power spectrum ratio of any two normal random time series with gaps using the LS method did not change this result (Figure S5A1 and A2). In contrast, the WWT method power spectrum results consistently met expectations with or without application of the alias filter. As a result, power spectral analysis of all time series data in this work was performed using the WWT method with alias filtering and spectral smoothing, as this constitutes the most conservative and robust (due to the increased degrees of freedom from smoothing) method.

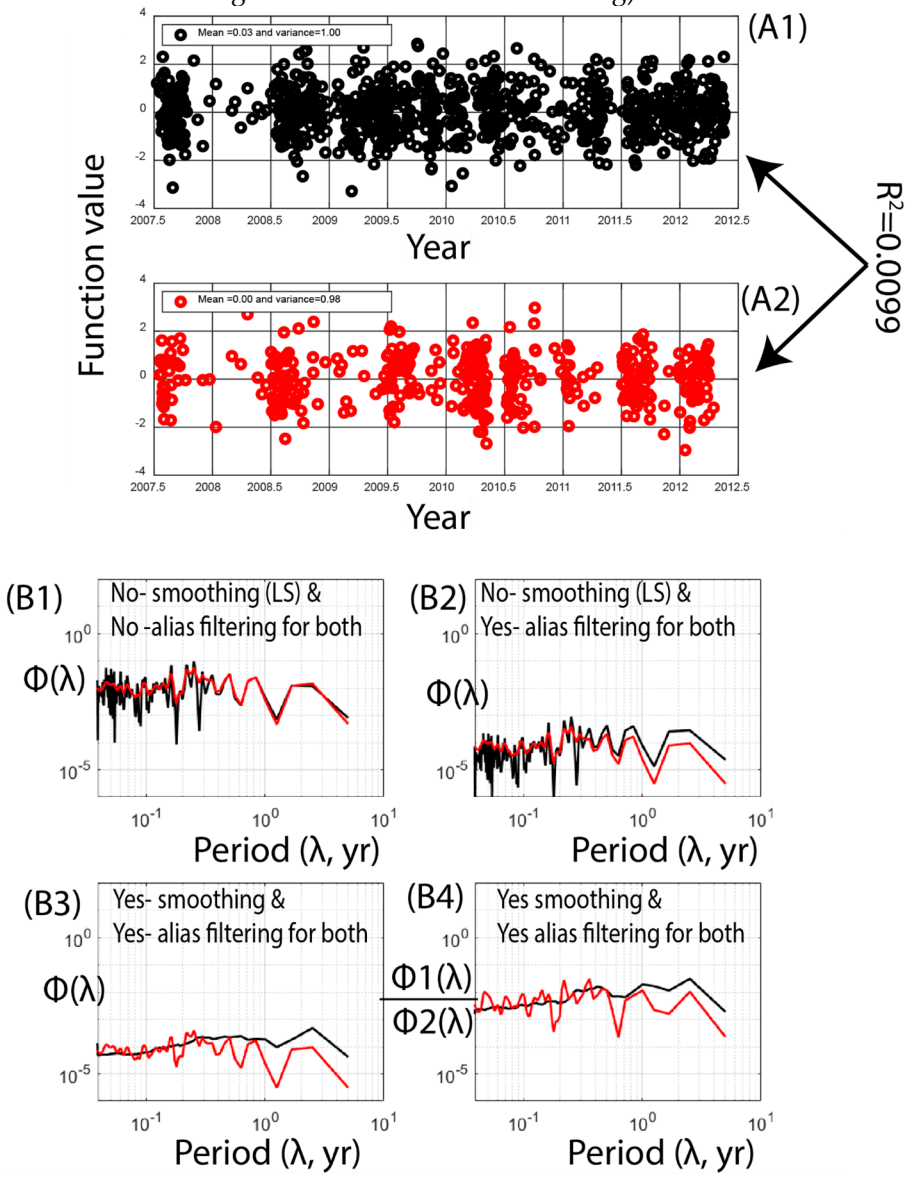

Figure S5. Effect of spectral smoothing and alias filtering on the power spectra of a continuous normal random time series (**A1**) using the Lomb-Scargle (LS; shown in black), and (**A2**) on another continuous normal random time series using the Weighted Wavelet Transform (WWT; shown in red) method. (**B1**) The power spectra generated with the LS and WWT methods when there is no power spectral smoothing for LS and no alias filtering for either method. (**B2**) The power spectra generated with the LS and WWT methods when there is no power spectral smoothing for LS, but alias filtering is used for both methods. (**B3**) The power spectra generated with the LS and WWT methods when both power spectral smoothing and alias filtering are performed with both methods. (**B4**) The ratio of the power spectra of time series A1 and A2 using LS (shown in black) and between time series A1 and A2 using

WWT (shown in red) when both power spectral smoothing and alias filtering are used for both methods. Note that the DFT method is only applicable on time series data without gaps, whereas the Lomb-Scargle method can accept time series data with gaps. For comparison, the time series A1 resembles our $\delta^{18}O$ time series in precipitation in terms of data gaps, and the time series A2 resembles our $\delta^{18}O$ time series in stream water in terms of data gaps.

S4. Effects of Time Series Transformation Using Equation (2) on the Estimated Phase Difference between Two Time Series

In the main text, we estimated the power spectrum of each component of the catchment-scale water balance equation using transformed (using Equation (2)) time series data. It is not clear, however, how time series transformation can or will affect its phase angle (or the terms ψ_i and ψ_j in Equations (5,6) for any period λ. For these reasons, we considered several synthetic time series', each created using:

$$A_i \sin\left(\frac{2\pi}{\lambda} t - \psi_i\right), \text{ with } A_i=1,\ \lambda = 1 \text{ yr} \quad \text{(S2)}$$

with known phase angle ψ_i, which varied from 0 to 350° (Figure S6A). Each time series with its transformed (using Equation (2) in the main text along with the median of the time series) and untransformed versions was then analyzed using the WWT method for the Fourier coefficients a_i and b_i. The phase angles (ψ_i) were predicted using:

$$\psi_i = \left(\frac{180}{\pi}\right)\left\{\arctan\left(\frac{-a_i(\lambda)}{b_i(\lambda)}\right)\right\}, \quad \text{(S3)}$$

where *arctan* is the standard inverse tangent function.

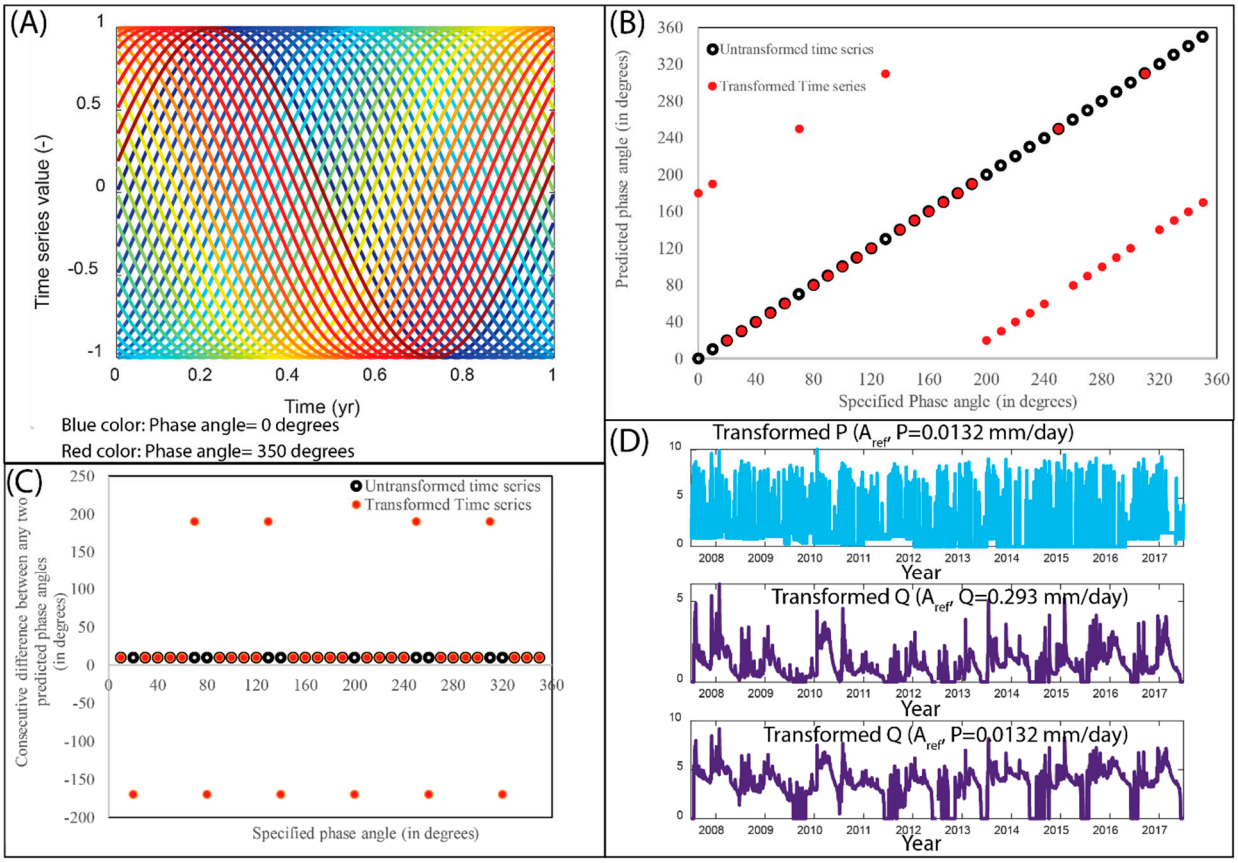

Figure S6. (**A**) Various synthetic sinusoidal time series. (**B**) A comparison of the specified and predicted phase angles when the time series data shown in (A) are untransformed (black hollow circles) and when they are transformed (red filled circles) using Equation (3) and the median value of each time series. (**C**) Consecutive differences between the predicted phase angles (untransformed: black hollow circles; transformed: red filled circles) at the specified phase angles. (**D**) Transformed

time series of precipitation (top plot) using its median value, streamflow using its median value (middle plot), and streamflow using the median value from the precipitation time series. For the precipitation and streamflow transformations shown in plot (D), Equation (2) was used.

The predicted phase angles for the untransformed time series were more reliable than the predicted angles using transformed time series data (Figure S6B). Note that for untransformed or transformed time series data, the phase angles or ψ terms in Equations 5 and 6 in the main text are predicted using Fourier coefficients for sinusoidal cycles with period = 1 year and using the WWT method in each case. Whereas the predicted phase angles with the transformed time series data did not always match the specified phase angles (red points in Figure S6B), the predicted phase angles with the untransformed time series matched the specified phase angles very closely (hollow points in Figure S6B). As a consequence, the phase angles were predicted using the untransformed time series data.

We tested the reliability of the predicted phase differences between any two transformed time series by considering their sinusoidal cycles (each with a period of 1 year). In this way, we calculated phase differences by using any two successive values of the predicted phase angles for untransformed and transformed time series data as a function of the specified phase angle for various sinusoidal cycles. The results demonstrate that the predicted phase differences between two transformed time series were not always correct (Figure S6C). Thus, our benchmarking exercise shows that a time series transformation can lead to unreliable predicted phase angles for a time series and unreliable phase differences between any two time series data sets.

In the previous benchmarking exercise, each time series was transformed using the median value of the corresponding time series, and there were no missing values or data gaps in any of the synthetic time series data. However, it is not clear how the predicted phase angle or the phase difference between any two transformed time series would change if each time series was transformed using the same reference value. Therefore, we tested two additional scenarios in which the same reference value was used for each time series transformation. For the first scenario, A_{ref} was set equal to -0.0032, and for the second scenario, A_{ref} was set equal to 0.0032, which are the median and absolute values of the median of the synthetic sinusoidal time series with a zero phase angle (Table S1).

When A_{ref} was positive and when it was consistently applied to each time series transformation, the predicted phase angles closely matched the specified phase angles (column 4 in Table S1). However, when A_{ref} was negative, the predicted phase angles differed from the specified phase angle by 180° (column 5 vs. column 1 in Table S1). Accordingly, we conclude that if the same positive reference value is used for each time series transformation, then the predicted phase angles for a time series or the phase differences between any two time series should be reliable. Notwithstanding, we caution against using the same reference value for transforming various time series data in order to predict their phase angles or phase angle differences between any data sets for the following reasons: (1) the main purpose of using the variance-equalizing function, i.e. Equation S1 above, is to equalize the variance of that time series with its own reference value and not with the reference value of another time series. (2) Further, each time series may have missing values and also different medians, and therefore the use of any particular median value for transforming multiple time series' is subject to error if the data gaps in each time series do not coincide (as is the case for various times series of hydrologic fluxes for MGC; see Figure 2). We illustrate the drawback of using the same reference value for normalizing various time series data in Figure S6D. When the reference value for transforming daily precipitation data (the transformed daily precipitation time series is shown by the top plot in Figure S6D) is used for transforming the daily streamflow data (bottom plot in Figure S6D), the resultant transformed time series no longer exhibits equal variance throughout the time series and it is also biased towards low values (Figure S6D bottom vs. middle plot).

Table S1. A comparison of predicted and specified (first column) phase angles when a time series is untransformed (column 2); when it is transformed using the median value of the corresponding time series (column 3); when it is transformed using the same positive reference value (A_{ref} = 0.0032) for

each time series (column 4); when it is transformed using the same negative reference value (A_{ref} = −0.0032) for each time series (column 5); the consecutive difference between two predicted phase angles when using the predicted phase angles from the untransformed time series (column 6); and when using the transformed time series along with the median value of the corresponding time series (column 7). TS is time series.

Specified angle (in degrees)	Predicted phase angles (in degrees)				Consecutive difference with untransformed TS	Consecutive difference with transformed time series with varying A_{ref}'s
	Untransf-ormed TS	Transformed TS	Transformed time series with A_{ref} = 0.0032 for all TS	Transformed time series with A_{ref} = −0.0032 for all TS		
0	0.00	180.01	0	180	Not applicable	Not applicable
10	9.96	189.88	10	190	9.96	9.86
20	19.92	19.87	20	200	9.96	-170.01
30	29.89	29.85	30	210	9.97	9.98
40	39.88	39.85	40	220	9.98	10.00
50	49.87	49.86	50	230	10.00	10.01
60	59.89	59.85	60	240	10.01	9.99
70	69.92	249.92	70	250	10.03	190.07
80	79.96	80.00	80	260	10.04	-169.92
90	90.00	90.01	90	270	10.04	10.01
100	100.04	100.04	100	280	10.04	10.03
110	110.08	110.07	110	290	10.04	10.03
120	120.11	120.08	120	300	10.03	10.01
130	130.12	310.12	130	310	10.02	190.03
140	140.12	140.23	140	320	10.00	-169.89
150	150.11	150.18	150	330	9.99	9.94
160	160.08	160.15	160	340	9.97	9.98
170	170.04	170.13	170	350	9.96	9.97
180	180.00	180.01	180	0	9.96	9.89
190	189.96	189.88	190	10	9.96	9.86
200	199.92	19.87	200	20	9.96	-170.01
210	209.89	29.85	210	30	9.97	9.98
220	219.88	39.85	220	40	9.98	10.00
230	229.87	49.86	230	50	10.00	10.01
240	239.89	59.85	240	60	10.01	9.99
250	249.92	249.92	250	70	10.03	190.07
260	259.96	80.00	260	80	10.04	-169.92
270	270.00	90.01	270	90	10.04	10.01
280	280.04	100.04	280	100	10.04	10.03
290	290.08	110.07	290	110	10.04	10.03
300	300.11	120.08	300	120	10.03	10.01
310	310.12	310.12	310	130	10.02	190.03
320	320.12	140.23	320	140	10.00	-169.89
330	330.11	150.18	330	150	9.99	9.94
340	340.08	160.15	340	160	9.97	9.98
350	350.04	170.13	350	170	9.96	9.97

S5. Comparison of Root Mean Square (RMS) Differences between Successive Local Averages for Stationary Versus Nonstationary Time Series Data

To better understand how the nature of a time series (stationary or non-stationary) affects the pattern of RMS differences between successive local averages (RMS differences), we considered two scenarios where we computed the RMS differences for synthetic stationary and non-stationary time

series data (Figure S7A1 for a stationary and B1 for a non-stationary data). The synthetic time series were generated using a second-order autoregressive AR (2) type model (Equation (S4)) [4].

$$x(t+1) = \mu + \theta_1\{x(t) - \mu\} + \theta_2\{x(t-1) - \mu\} + \varepsilon(t+1), \quad \text{(S4)}$$

where θ_1 and θ_2 are the first and second parameters of the AR (2) model, μ is the mean value of the synthetic time series, and $\varepsilon(t+1)$ is a normal random number with mean zero and variance one. We selected x(t = 1 day) = x(t = 2 day) = 0.5 and $\mu = 0$ for both the stationary and non-stationary time series, along with $\theta_1 = 0.9$ and $\theta_2 = -0.6$ for the stationary time series and $\theta_1 = 0.9$ and $\theta_2 = 0.1$ for the non-stationary time series. The parameter $\varepsilon(t+1)$ in Equation S4 was generated using the MATLAB® function normrnd with a mean of 0 and variance of 1. The length of the time series was the total number of daily time steps between calendar years 2007 and 2017. The synthetic time series data are shown in Figure S7A1 (stationary) and B1 (non-stationary). To ensure the consistency of the RMS difference estimation method between the synthetic stationary and non-stationary time series data, we intentionally deleted data from both time series to create data gaps at the same time periods when data gaps exist in the daily precipitation (stationary time series) or streamflow (non-stationary) data, respectively.

Our results show that the stationary time series exhibited self-averaging behavior, whereas there was evidence of fractal or power-law behavior for the non-stationary time series (Figure S7A2 and B2). The RMS differences for the stationary time series approached the expected slope (shown in red in Figure S7A2) for a time series with self-averaging behavior, i.e., the mean of the time series gradually approached a stable value as the averaging interval size increased. In contrast, the RMS differences for the non-stationary time series increased with the averaging time scale (Figure S7B2). These results suggest self-averaging behavior at higher temporal averaging scales for the stationary time series and power-law behavior across temporal scales for the non-stationary time series.

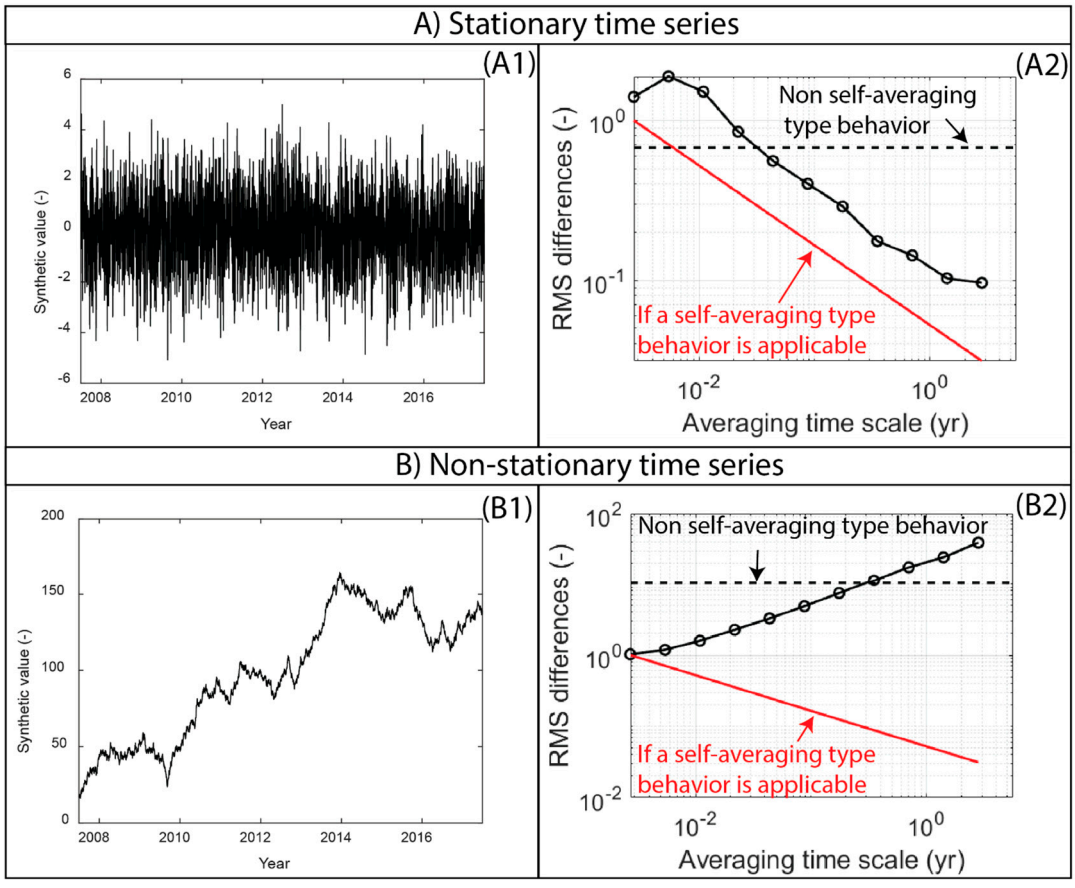

Figure S7. A stationary time series (**A1**) and the corresponding pattern of root mean square (RMS) differences between successive local averages across various temporal averaging scales (**A2**). A non-

stationary time series (**B1**) and the corresponding pattern of root mean square (RMS) differences between successive local averages across various temporal averaging scales (**B2**). The horizontal lines in plots A2 and B2 indicate a non-self-averaging type behavior with a slope of zero between RMS differences and the logarithmic temporal averaging scales. The red line in plots A2 and B2 with a log-scale slope of -0.5 indicates the expected behavior for a self-averaging time series from the application of the central limit theorem [5].

S6. Sensitivity Analysis of the Effect of ET Corrections on the AET Power Spectrum

We corrected observed evapotranspiration (ET) at the Mt. Bigelow flux tower to AET using the water balance method with the assumption that total change in fractured bedrock storage for any water year is zero (Figure S8A). Subsequently, we performed a sensitivity analysis of the ET power spectrum because it was unknown how corrections in the observed flux tower ET data may affect the power spectrum of the resultant AET time series. In this analysis, we estimated the power spectra of the ET (black curve in Figure S8A) and AET time series data between WY 2010 and WY 2017. The results (Figure S8B) show similarities between the ET and AET power spectra with peaks and troughs at similar times. Note that before this sensitivity analysis, each ET time series was variance-equalized using Equation (S1) above. The A_{ref} was estimated as the median value of each time series during the measurement period.

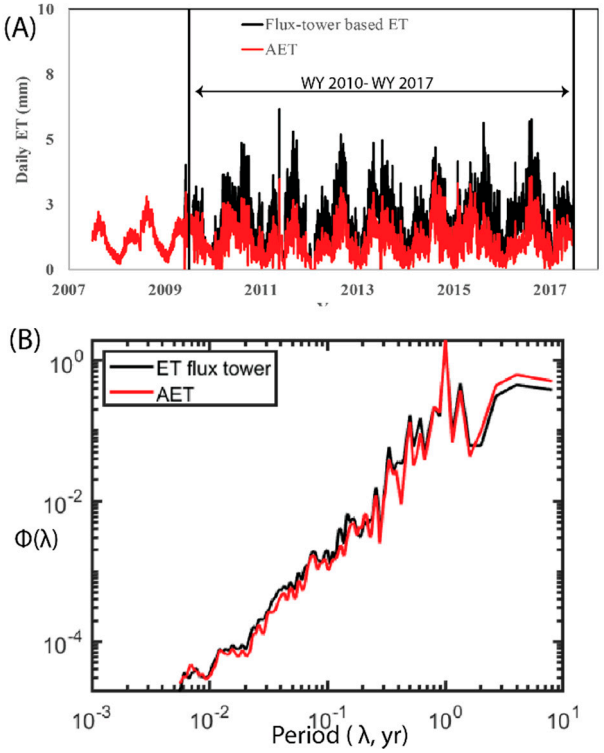

Figure S8. (**A**) Time series plot of flux-tower based ET (black solid line) and AET (red solid line) time series data from WY 2008 to WY 2017. (**B**) Comparison of the ET and AET power spectra. The two vertical black solid lines in (A) mark the spectral analysis period.

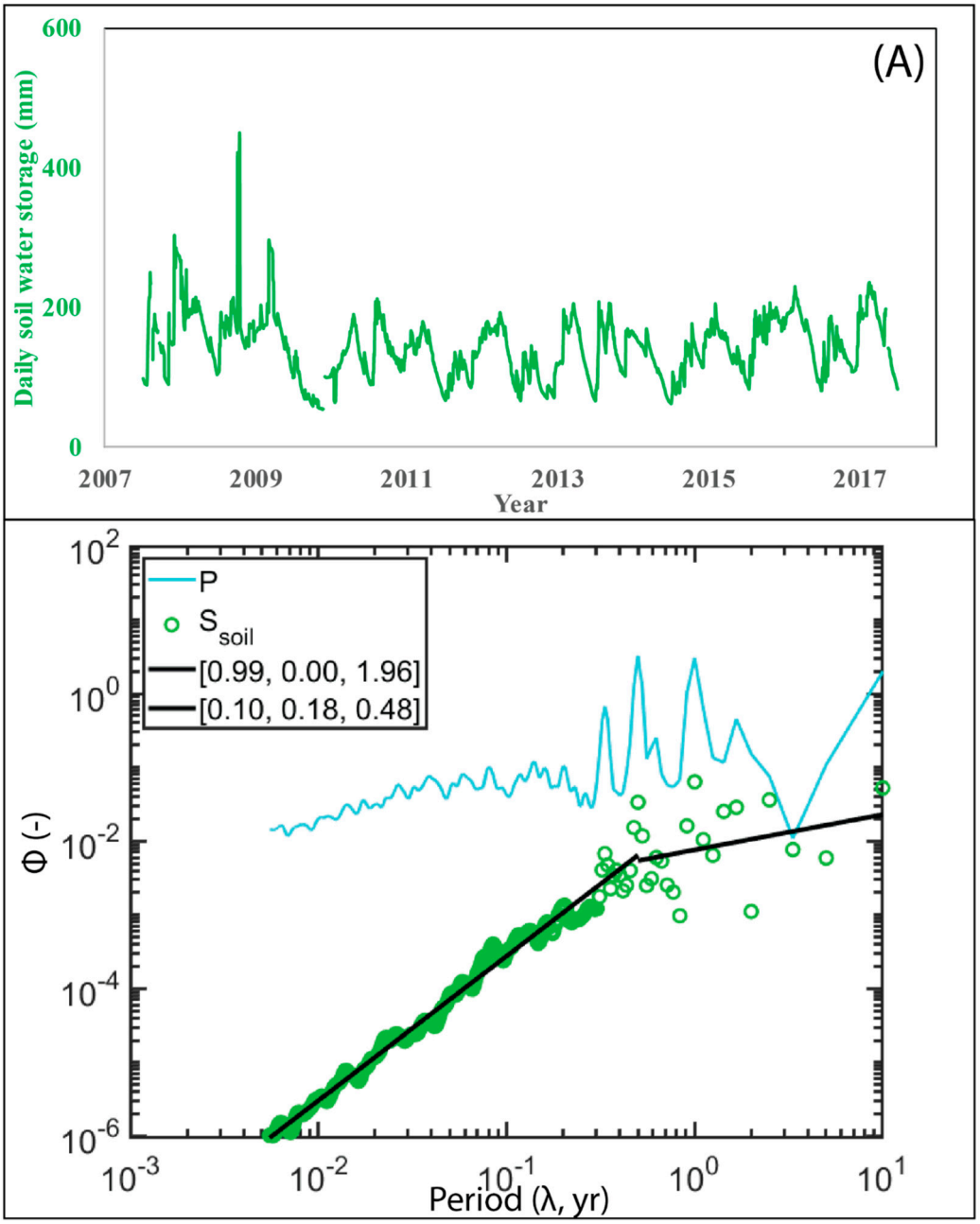

Figure S9. Time series of daily soil water storage (**A**). The power spectrum of the transformed daily soil water storage along with the regression line (**B**). Transformation of the soil water storage time series was performed using Equation (2) in the main text with A_{ref} equal to the median value between WY 2008 and WY 2017. The light blue curve in (B) shows the precipitation power spectrum for the same period range; triplets for the fitted lines in (B) represent (R^2, p-value, and the fractal slope).

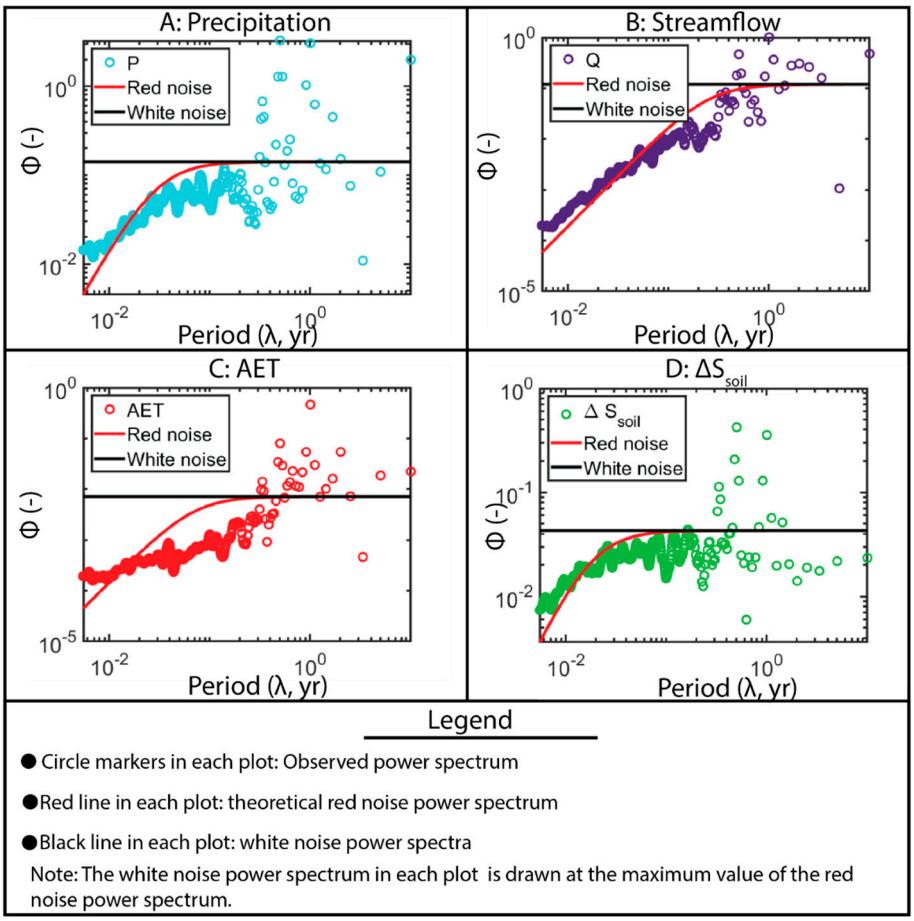

Figure S10. Observed power spectra for various components of the water balance equation using hydrologic fluxes and storages between water years 2008 and 2017. In each plot the black solid curve shows the white noise spectrum and the red solid curve shows the theoretical red noise power spectrum.

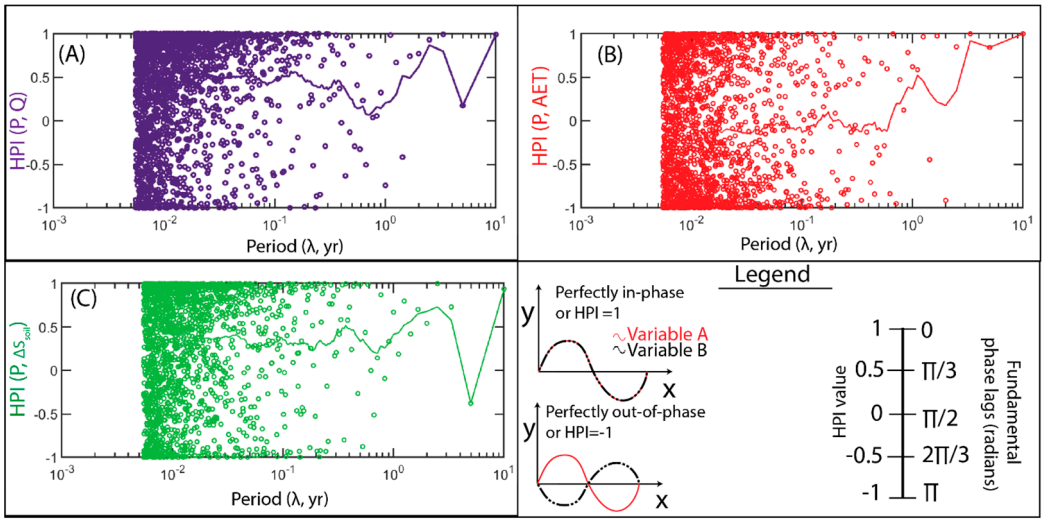

Figure S11. The period-dependent Hydrologic Phase Index (HPI) between precipitation (P) and (**A**) streamflow, (**B**) AET, and (**C**) the daily change in soil water storage (ΔS_{soil}). The hollow points and solid curves in each plot show the spectrally un-smoothed and smoothed HPI spectra (see Section 3.3 in the main text for more details).

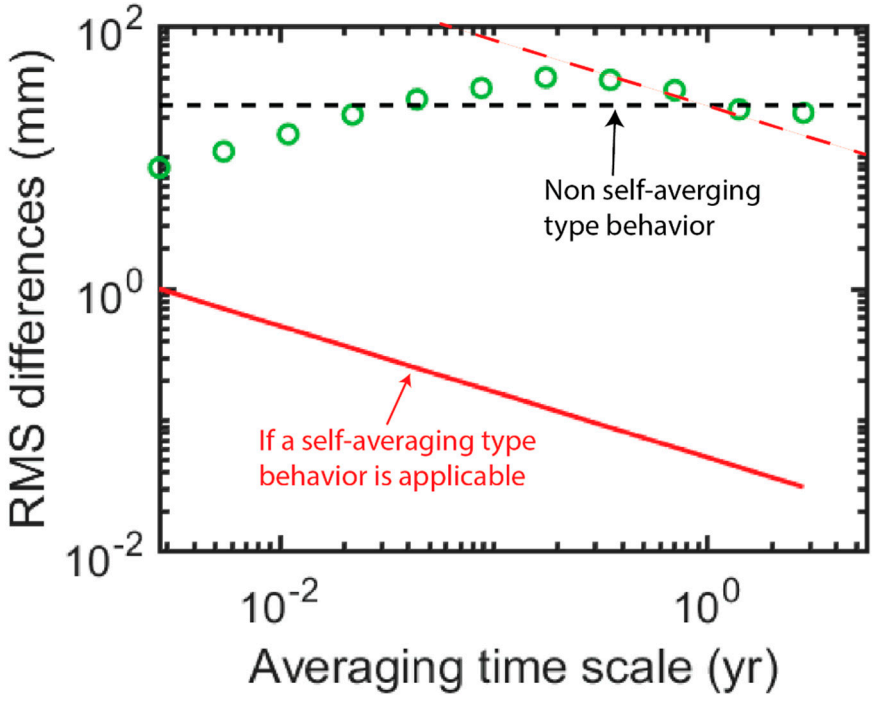

Figure S12. Root mean square differences between successive local averages for daily soil water storage as a function of averaging time scale. The horizontal dashed line indicates non-self-averaging type behavior and the solid red line with a slope of -0.5 on a log-sale indicates the expected behavior for a self-averaging type time series from the application of the central limit theorem [5].

References

1. Dickinson, J.E.; Hanson, R.T.; Predmore, S.K. HydroClimATe—Hydrologic and Climatic Analysis Toolkit; USGS: 2014; p 49.
2. McKee, T.B.; Doesken, N.J.; Kliest, J. The relationship of drought frequency and duration to time scales. In Proceedings of 8th Conference of Applied Climatology, Anaheim, CA, USA, 17–22 January 1993.
3. Edwards, D.C. Characteristics of 20th century drought in the United States at multiple time scales Colorado State University, Fort Collins, CO, USA, 1997.
4. Wilks, D.S. Stochastic methods in atmospheric sciences, 3rd ed.; Academic Press: 2011; Vol. volume 100.
5. Kirchner, J.W.; Neal, C. Universal fractal scaling in stream chemistry and its implications for solute transport and water quality trend detection. Proceedings of the National Academy of Sciences of the United States of America 2013, 110, 12213–12218, doi:10.1073/pnas.1304328110.
6. Kirchner, J.W. Aliasing in 1/f(alpha) noise spectra: origins, consequences, and remedies. Physical review. E, Statistical, nonlinear, and soft matter physics 2005, 71, 066110, doi:10.1103/PhysRevE.71.066110.
7. Kirchner, J.W.; Feng, X.; Neal, C. Fractal stream chemistry and its implications for contaminant transport in catchments. *Nature* **2000**, *403*, 524–527.
8. Godsey, S.E.; Aas, W.; Clair, T.A.; de Wit, H.A.; Fernandez, I.J.; Kahl, J.S.; Malcolm, I.A.; Neal, C.; Neal, M.; Nelson, S.J., et al. Generality of fractal 1/f scaling in catchment tracer time series, and its implications for catchment travel time distributions. *Hydrol. Processes* **2010**, *24*, 1660–1671, doi:10.1002/hyp.7677.